CaCl and CaF emission in LIBS under simulated Martian conditions

D. S. Vogt[a], S. Schröder[a], K. Rammelkamp[a], P. B. Hansen[a], S. Kubitza[a], H.-W. Hübers[a,b]

[a] *Deutsches Zentrum für Luft- und Raumfahrt e.V. (DLR), Institut für Optische Sensorsysteme, Berlin, Germany*
[b] *Humboldt-Universität zu Berlin, Institut für Physik, Berlin, Germany*

Abstract

Chlorine and fluorine play an important role in the geological history of Mars due to their high concentration in Martian magmas and their influence on the generation and evolution of Martian basalts. Chlorine-bearing salts could also facilitate the formation of eutectic brines that could be important for the fluvial history of Mars. The LIBS instruments of ChemCam and SuperCam can detect emission lines of Cl and F, but the intensity of these emission lines is comparatively low, making it difficult to quantify them correctly. A promising alternative is the quantification by molecular emission of diatomic molecules like CaCl and CaF, which can be observed as intense molecular bands in LIBS spectra if Ca is also present. However, the nonlinear dependence of the band intensity on the concentrations of both elements needs to be considered. In this study, we expand upon our previous analysis of molecular bands by investigating samples which produce CaCl bands, CaF bands, or both. We find that the highest CaCl band intensities are found in samples containing more Ca than Cl, while the strongest CaF bands are found in samples with roughly equal concentrations of Ca and F. Both observations can

be described by the model that we present here. We also find that the CaCl band is significantly stronger for a sample containing $CaCl_2$ than it is for a sample containing the same concentrations of Ca and Cl in separate bonds. The opposite is true for the CaF band, which is significantly weaker for the sample containing CaF_2 bonds than it is for the sample that does not contain CaF_2 bonds. These matrix effects are partially attributed to fragmentation during the ablation process and differences in the dissociation energies. Furthermore, we observe that CaF formation is not affected by competing CaCl formation, while CaCl is strongly affected by competing CaF formation. All measurements are done in simulated Martian atmospheric conditions in order to assist the analysis of Martian LIBS data.

Keywords: Mars, Spectroscopy, Experimental techniques

---

1. Introduction

The ChemCam instrument suite (Maurice et al., 2012; Wiens et al., 2012) on board the NASA Mars Science Laboratory plays a vital role in the geological analysis of the Martian surface at Gale crater. It employs laser-induced breakdown spectroscopy (LIBS), a type of atomic emission spectroscopy that uses a pulsed high-energy laser to create a plasma plume that emits light from mostly atomic and ionic transitions (Cremers and Radziemski, 2006). With LIBS, ChemCam can analyze targets at stand-off distances between 1.3 m and 7 m (Maurice et al., 2012). No sample preparation is required and only a small part of the sample is ablated, making it minimally invasive. Since the start of the mission in 2012, ChemCam has acquired more than 600,000 spectra, enabling the qualitative and quantitative analysis of major, minor,

and trace elements on the Martian surface (Maurice et al., 2016). It was also the first instrument to detect the elements fluorine and boron on Mars (Forni et al., 2015; Gasda et al., 2017).

ChemCam's quick stand-off analysis is helpful for the selection of samples for the contact and analytical laboratory instruments of the Mars Science Laboratory (Grotzinger et al., 2012). In addition to LIBS spectra of selected targets, it also provides high-resolution images with the integrated Remote Micro-Imager (RMI), which help to contextualize the measurements (Nachon et al., 2014; Le Mouélic et al., 2015; Maurice et al., 2012). A successor instrument of ChemCam called SuperCam will be part of NASA's Mars 2020 mission. SuperCam will again employ stand-off LIBS, but it will also be able to perform stand-off Raman spectroscopy, visible and infrared reflectance spectroscopy, and luminescence spectroscopy (Wiens et al., 2017).

The detection of chlorine and fluorine with ChemCam and SuperCam is important due to their key role in the geological and aqueous history of Mars. Apatites and amphiboles in SNC meteorites contain more Cl and F than OH, indicating high concentrations of Cl and F in the Martian parental magmas (Filiberto and Treiman, 2009a; Filiberto et al., 2016). It has been proposed that Cl could be the dominant volatile in Martian magmas instead of water (Filiberto and Treiman, 2009a), and that it plays a crucial role in the generation and evolution of Martian basalts by lowering the liquidus temperature (Filiberto and Treiman, 2009b). Furthermore, perchlorates and chlorides have been detected on Mars (Hecht et al., 2009; Massé et al., 2010; Osterloo et al., 2010), which could produce eutectic brines that are liquid at the low temperatures of present Mars (Burt and Knauth, 2003; Möhlmann

and Thomsen, 2011; Clark and Kounaves, 2016). The first detection of F on Mars was made possible by ChemCam, which revealed many fluorine-bearing phases that were proposed to be micas, amphiboles, apatites, topaz, or fluorite (Forni et al., 2015). The detected high concentrations of F of several wt% in igneous rocks could indicate that F is as important as Cl, or even more important, in basalt formation and mantle melting, since it has a similar effect on basaltic liquidus depression (Filiberto et al., 2012).

In LIBS measurements, the detection and quantification of Cl and F by atomic or ionic emission lines is challenging. One of the main reasons for this is that the distribution of the energy levels in Cl and F produces strong emission lines in the vacuum ultraviolet (VUV) spectral range, but only weak emission lines in the typically applied spectral range, cf. ChemCam (242 nm to 900 nm). Molecular emissions of CaCl and CaF can improve the detection of Cl and F (Gaft et al., 2014; Alvarez-Llamas et al., 2016; Vogt et al., 2018). These diatomic molecules, which form in the laser-induced plasma if Ca is present along with Cl or F, produce intense molecular bands even at low concentrations of Cl or F. Indeed, the first detection of F on Mars was made possible by CaF emissions (Forni et al., 2015; Meslin et al., 2016).

While the detection of chlorine and fluorine can be improved by molecular emissions of CaCl and CaF, the quantitative analysis is more challenging. Since both components of the diatomic molecule need to be present in the plasma in sufficient concentrations, the molecular band intensities exhibit a nonlinear behavior, as shown in our last study on CaCl emission (Vogt et al., 2018). The CaCl band intensity was found to be more dependent on the Ca concentration than on the Cl concentration, resulting in maximum

intensities if there is more Ca in the sample than Cl. For specific samples, diatomic molecules in the laser-induced plasma can also be formed from the vaporization of solid fragments ejected from the sample matrix during ablation (Perez and Lewis, 2002; Doucet et al., 2008). In the case of CaCl and CaF, formation by fragmentation would be mostly expected for samples containing $CaCl_2$ and CaF_2, so that the emission intensity might differ between samples containing these bonds and those that do not. Finally, if all three elements Ca, Cl, and F are present in the same sample, e.g. in apatites ($Ca_5(PO_4)_3(F, Cl, OH)$) containing different proportions of F, Cl or OH anions, the intensities of both CaCl and CaF emission might be reduced because of the competing formation of both molecules.

In the present study, we analyze the molecular emissions of CaCl and CaF in simulated Martian atmospheric conditions. The dependence of the band intensities on the reactant concentrations is analyzed and a theoretical description is derived based on the chemical reactions in the laser-induced plasma. The influence of the initial bonds in the sample matrix and of the formation of competing diatomic molecules is investigated as well. Since the atmospheric conditions strongly affect the lifetime and intensity of the laser-induced plasma (Knight et al., 2000), our results are very specific for the Martian environment and therefore relevant for current and future Martian LIBS data.

2. Methods

2.1. Samples and experiments

Pure and mixed samples made from seven different salts (K_2SO_4, $CaCO_3$, KCl, MgF_2, CaF_2, $CaSO_4 \cdot 2\,H_2O$, and $CaCl_2 \cdot 2\,H_2O$) were used in this study. All salts used in this study are reagent-grade. In total, five different series were made. Table 1 gives an overview of the samples, categorized by test series and by experiment, and shows which laser energies were used for the measurements. Three fundamental experiments (A, B, C) were conducted for this study. In each case, the influence of the sample composition (or the chemical matrix) on the intensity of the molecular emissions is investigated. In order to obtain suitable and explicable trends, all elemental quantities are converted from weight percentages to molar fractions or atomic percentages, in accordance with the recommendation by Hahn and Omenetto (2012).

A: Dependence on reactant concentrations. Here we study the dependence of the molecular emission on the concentrations of the two reactants, namely calcium and chlorine or calcium and fluorine. Two separate sets of samples with anti-correlated concentrations of the reactants were made for this experiment. The first set is for the investigation of the CaCl band in dependence of the Ca and Cl content in the samples. It consists of 20 samples, in which the sum of the molar fractions of Ca and the Cl is kept constant at $\chi_{\mathrm{Ca}} + \chi_{\mathrm{Cl}} = 0.2$ (20 at%). This is achieved by mixing a 1:1 mass mixture of K_2SO_4 and KCl ("Mix 1", $\chi_{\mathrm{Cl}} = 0.2$) with $CaCO_3$ ($\chi_{\mathrm{Ca}} = 0.2$) at different ratios. This test series is the *CaCl band series*.

The second series is for the equivalent investigation of the CaF band intensity and its dependence on the Ca and F concentrations. Again, the

Table 1: Overview of the test series made for this study, showing the fundamental formulae for the mixtures and for the molar fractions of the investigated reactants Ca, Cl, and F. The variables α and β indicate varying weight fractions of the substances in the mixtures. Mix 1 is a 1:1 mixture of K_2SO_4 and KCl and Mix 2 is a 2.8:1 mixture of K_2SO_4 and MgF_2.

Series	Mixture	Molar fractions (Ca, Cl, F)	# samples	Experiment	Laser energy (mJ/pulse)
CaCl band series	$\alpha\,\text{Mix 1} + (1-\alpha)\,CaCO_3$	$\chi_{Ca} = 0 \ldots 0.2$, $\chi_{Cl} = 0.2 - \chi_{Ca}$	20	A	17, 23, 35
CaF band series	$\alpha\,\text{Mix 2} + (1-\alpha)\,CaCO_3$	$\chi_{Ca} = 0 \ldots 0.2$, $\chi_{F} = 0.2 - \chi_{Ca}$	15	A	17, 23, 35
Initial bond series	(different mixtures)	$2\chi_{Ca} = \chi_{Cl} = 0.222$ or $2\chi_{Ca} = \chi_{F} = 0.250$	4	B	23, 35
CaF robustness series	$\alpha\,CaF_2 + \beta\,KCl + (1-\alpha-\beta)\,K_2SO_4$	$2\chi_{Ca} = \chi_{F} = 0.03$, $\chi_{Cl} = 0 \ldots 0.087$	15	C	23
CaCl robustness series	$\alpha\,CaCl_2 \cdot 2\,H_2O + \beta\,MgF_2 + (1-\alpha-\beta)\,K_2SO_4$	$2\chi_{Ca} = \chi_{Cl} = 0.03$, $\chi_{F} = 0 \ldots 0.155$	9	C	23

sum of the molar fractions of Ca and F is kept constant at $\chi_{Ca} + \chi_F = 0.2$ (20 at%), this time by mixing a 2.8:1 mass mixture of K_2SO_4 and MgF_2 ("Mix 2", $\chi_F = 0.2$) with $CaCO_3$. This series is the *CaF band series*. It consists of 15 samples, as the results of the CaCl band series indicated that a smaller sample size would be sufficient.

B: Dependence on the initial bond. It is expected that the existing bonds in the sample matrix have an effect on the molecular emission if not all bonds are broken up during plasma formation. If Ca and Cl are bonded as $CaCl_2$, for example, fragmentation might cause CaCl or $CaCl_2$ molecules or larger fragments of the $CaCl_2$ crystal to be present in the plasma. This can significantly change the CaCl formation process in comparison to the alternative, in which three-body reactions via random collisions of Ca and Cl atoms and a

third body are necessary (see section 3.2). In order to test this, four samples were made, which are called the *initial bond series*. Two of the samples contain the same concentrations of Ca and Cl, but in different chemical bonds. The first sample is made from pure $CaCl_2 \cdot 2\,H_2O$, while the second sample is obtained from a mixture of 59.7 wt% KCl and 40.3 wt% $CaCO_3$. They both contain 11.1 at% Ca and 22.2 at% Cl ($\chi_{Ca} = 0.111$, $\chi_{Cl} = 0.222$). The next two samples both contain 12.5 at% Ca and 25.0 at% F ($\chi_{Ca} = 0.125$, $\chi_F = 0.250$). Again, one sample contains initial bonds between the two elements, while the other does not. The first sample consists of 38.6 wt% CaF_2 and 61.4 wt% K_2SO_4, and the second sample consists of 38.4 wt% MgF_2 and 61.6 wt% $CaCO_3$.

C: Influence of competing reactants. If both Cl and F are present in the plasma, then CaCl formation and CaF formation are in direct competition with one another. This should affect the intensity of both molecular emissions. In order to study this effect, two sets of samples were made. In the first series, called the *CaF robustness series*, the concentrations of Ca and F were kept at a constant 1:2 ratio and at a nearly constant value, while Cl was added in different concentrations. For the samples CaF_2 was mixed with KCl and K_2SO_4, while keeping the concentrations of Ca and F close to 1.5 at% and 3 at%, respectively. The Cl concentration varies from 0 at% to 8.7 at%. 15 samples were made for this series. In the second series, called the *CaCl robustness series*, $CaCl_2 \cdot 2\,H_2O$ was mixed with MgF_2 and K_2SO_4. The Ca and Cl concentrations in these samples were close to 1.5 at% and 3 at%, respectively, while the F concentration varied from 0 at% to 15.5 at%. The number of samples was reduced to nine, while the highest F concentra-

tion was adjusted to be about five times higher than the Cl concentration, in order to investigate its influence over a wider range.

Sample preparation. Mixed samples were made using a scientific scale (uncertainty $\Delta m < 0.01\,\mathrm{g}$). Due to the importance of having specific values for the elemental concentrations, which can quickly change even for small variations of the masses, the mixing process had to be done very carefully. Uncertainties in the molar fractions were calculated from the weight measurements of the individual substances and the uncertainty of the scale. After mixing the components, the samples were ground into a fine powder using a mortar and pestle. Then they were pressed into pellets of about 1 g by applying a pressure of 0.25 GPa for 10 minutes.

2.2. Experimental setup

Measurements were made with the LIBS system at the Institute of Optical Sensor Systems of the German Aerospace Center (DLR) that was already described in previous publications (Schröder et al., 2013; Vogt et al., 2018; Schröder et al., 2019). It features a low-pressure simulation chamber with a motorized sample stage, an echelle spectrometer and several pulsed laser sources. The echelle spectrometer (LTB Aryelle Butterfly) uses a time-gated intensified charge-coupled device (ICCD) camera (Andor iStar), which can be time-gated in steps of 10 ns. For this study, the delay time between laser pulse and the start of the measurement was set to 350 ns and the gate width was set to 10 µs. These time settings were found to be beneficial because the continuum emission in the first plasma stage is omitted and because there is no significant plasma emission after 10 µs at Martian pressure (Vogt et al.,

2018). The Aryelle Butterfly can be switched between two spectral ranges: ultraviolet (UV) from 190 nm to 350 nm, and ultraviolet/visible/near-infrared (UV/VIS/NIR) from 270 nm to 850 nm. The UV/VIS/NIR spectral range was used for this study. It has a spectral resolution of about 0.03 nm full width at half maximum (FWHM) in the UV to about 0.09 nm FWHM in the NIR.

We used a Q-switched Nd:YAG laser with a wavelength of 1064 nm and a pulse width of 6 ns. The pulse energy was set to 17 mJ, 23 mJ, or 35 mJ. The pulse energy was varied in order to investigate the influence of the associated change of plasma parameters like temperature and electron density on the band intensity. For all measurements, the signal of 30 successive laser shots was integrated for a single spectrum in order to improve the signal-to-noise ratio. Each sample was measured at 10 different positions for improved accuracy and for the calculation of the standard deviation. The simulation chamber was filled with Mars-analog atmosphere (95.55 vol% CO_2, 2.7 vol% N_2, 1.6 vol% Ar, and 0.15 vol% O_2) at a pressure of 650 Pa for all measurements in order to be close to Martian atmospheric conditions (Harri et al., 2014).

3. Results

3.1. General characteristics of the CaCl and CaF band series

Spectra. Fig. 1 shows the spectra of pure $CaCO_3$, Mix 1, and Mix 2, averaged from 10 measurements of each sample. The spectra shown here were all obtained with a laser pulse energy of 35 mJ. For the $CaCO_3$ sample, strong lines of Ca(I) and Ca(II) dominate the spectrum. A slight contamination with

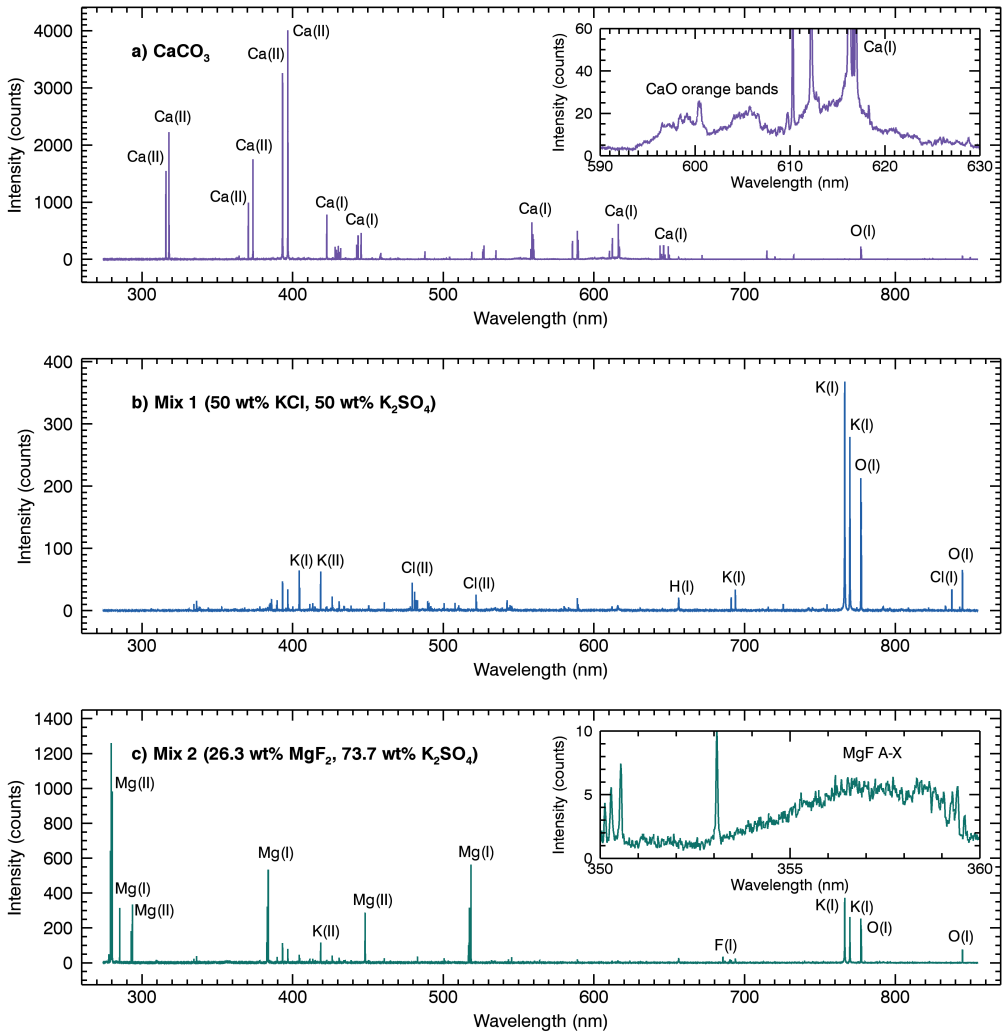

Figure 1: LIBS spectra of (a) $CaCO_3$, (b) Mix 1, and (c) Mix 2 showing characteristic emission lines. The $CaCO_3$ spectrum features the orange system of CaO bands between 590 nm and 630 nm. In the spectrum of Mix 2, a weak MgF $A^2\Pi_r - X^2\Sigma^+$ band can be observed. The spectra have been averaged from 10 measurements per sample. Each measurement was integrated over 30 laser shots. The laser pulse energy was 35 mJ.

Na can also be seen, most clearly from the Na(I) line doublet at 589.0 nm and 589.6 nm. The orange bands of CaO appear between 593 nm and 630 nm (see inset) (Marks et al., 1982). They are not superimposed by bands from other molecules yet, but will be superimposed by the $A^2\Pi - X^2\Sigma^+$ bands (A-X bands) of both CaF and CaCl in the spectra of mixed samples. In order to distinguish between the CaO bands and the superimposed CaF and CaCl bands, the band system of CaO seen in this spectrum is later used as one of three reference spectra in order to obtain the separate intensities of CaO, CaCl, and CaF. The other two reference spectra are those of nearly pure CaF and CaCl bands, respectively. By fitting a linear combination of these reference spectra to the measured spectra in experiments A, B, and C, the three band intensities are obtained. The Ca(I) lines at 610 nm, 612 nm, 616 nm, and 617 nm were masked so that they did not influence the intensity calculation.

In the spectrum of Mix 1, emission lines of Cl(I) and Cl(II) can be observed along with strong K(I) and K(II) lines. The spectrum of Mix 2 shows emission lines of F(I) along with strong lines of Mg(I) and Mg(II). There are also K(I) and K(II) lines, but they are less pronounced than in Mix 1, as expected due to the lower concentration of K_2SO_4. Additionally, the MgF $A^2\Pi_r - X^2\Sigma^+$ band can be observed between 353 nm and 360 nm (see inset). The band is too weak to be useful for the detection of fluorine, with a maximum intensity that is 5.8 times lower than that of the F(I) line at 685.6 nm. Furthermore, it cannot be detected by ChemCam and SuperCam due to a gap in the spectral range from 340 nm to 380 nm. For the following experiments, the low MgF band intensity means that the results will not be

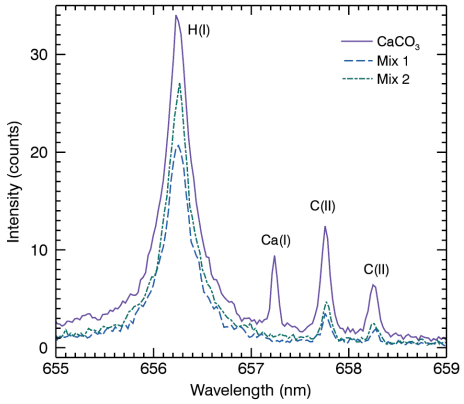

Figure 2: H_α line and C(II) lines in $CaCO_3$, Mix 1, and Mix 2. In the spectrum of $CaCO_3$, a Ca(I) also appears close to the H_α line. The Stark broadening of the H_α line can be used for the calculation of electron densities. As the width of the line does not change significantly for the different samples, the calculated electron densities are also very similar.

significantly affected by MgF formation.

A strong signal that appears in all three spectra is the O(I) triplet at 777 nm. Even though there is more oxygen in the $CaCO_3$ sample (60 at% in comparison to 34 at% and 40 at% in Mix 1 and Mix 2, respectively), the intensity of the triplet does not change significantly. This indicates that the oxygen from the CO_2 atmosphere strongly dominates the emission, cf. (Gasnault et al., 2012; Beck et al., 2017). Other signals that appear in all three spectra include the H_α line at 656.3 nm (Fig. 2), which is probably mostly caused by adsorbed water in the samples, and the two weak C(II) lines at 657.8 nm and 658.3 nm. The C(II) lines are always present due to the CO_2-dominant Martian atmosphere, but they can be observed especially well in $CaCO_3$, which provides additional carbon. A weak Ca(I) line appears

close to the H_α line in the $CaCO_3$ spectrum as well. In spectra of ChemCam or SuperCam, which have a lower resolution of about 0.65 nm FWHM at this wavelength (Wiens et al., 2012), this Ca(I) line will be indistinguishable from the H_α line, since the C(II) lines already cannot be clearly distinguished from the H_α line. To our knowledge, the potential interference of this Ca(I) line has not been considered before in ChemCam studies on hydrogen (Schröder et al., 2015; Rapin et al., 2016).

Even though there is a high amount of carbon available (20 at% in $CaCO_3$), the bands of C_2 cannot be observed in any of these spectra. The Swan system, the most common band system of C_2, has been observed under Martian atmospheric conditions for carbon-bearing samples before (Ollila et al., 2011). However, it is possible that the formation of carbon monoxide is favored over the formation of diatomic carbon if enough oxygen is available. Indeed, the dissociation energy of CO is 11.1 eV, while the dissociation energy of C_2 is only 6.2 eV (Radzig and Smirnov, 1985), which makes the formation of CO much more likely. In this case, C_2 would only appear in Martian LIBS spectra under very specific conditions, e.g. for graphite targets or organic compounds with low amounts of oxygen.

The spectra of the mixed samples mostly consist of the lines of the two components of the mixture, but the CaCl bands and the CaF bands appear as well (Fig. 3). The most intense band system is the $A^2\Pi - X^2\Sigma^+$ system, of which the most intense spectral feature is actually a superposition of the bands within the $\Delta\upsilon = 0$ band sequence, i.e. bands from transitions with no change in the vibrational quantum number υ (Asundi, 1935). The $\Delta\upsilon = 0$ band sequence of the $A^2\Pi - X^2\Sigma^+$ system will simply be called the A-X band

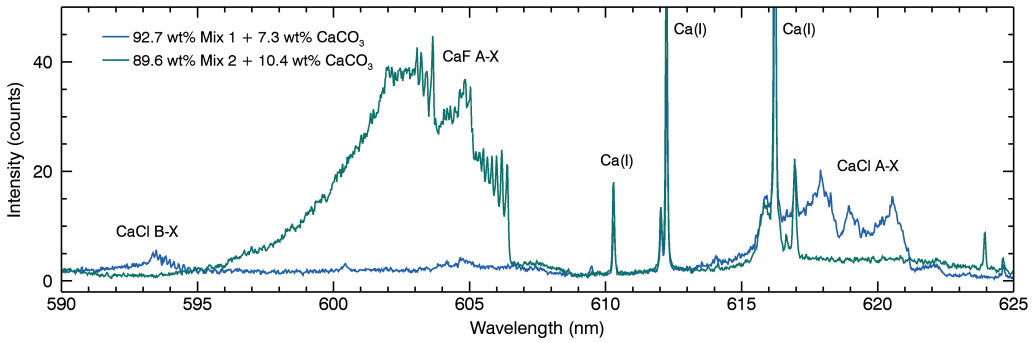

Figure 3: Spectra of mixed samples showing the molecular bands CaF and CaCl investigated in this study. Both spectra have been averaged from all 10 measurements on a sample.

in the following. For CaCl this A-X band appears at 615–621 nm, for CaF it is located at 595–607 nm. The second-most intense spectral features of CaCl and CaF are the B-X bands, i.e. the strongest band sequences of the $B^2\Sigma - X^2\Sigma^+$ system, located at 590–596 nm for CaCl and at 529–540 nm for CaF. Since no significant difference between the behavior of the A-X bands and the B-X bands could be observed, only the more intense A-X bands are investigated in this study.

The spectra in Fig. 3 are from samples with low concentrations of Ca, but high concentrations of Cl and F (2.1 at% Ca and 18.3 at% Cl for the CaCl band spectrum, 2.4 at% Ca and 17.6 at% F for the CaF band spectrum). Thus, the intensity of the CaO bands is close to zero, whereas the intensities of the CaCl band and the CaF band are comparatively high. Despite the nearly equal concentrations of Cl and F in these samples, the CaF band has a higher intensity than the CaCl band, while also showing very typical comb-like peaks close to 606 nm and a profile that is degraded to the violet. By

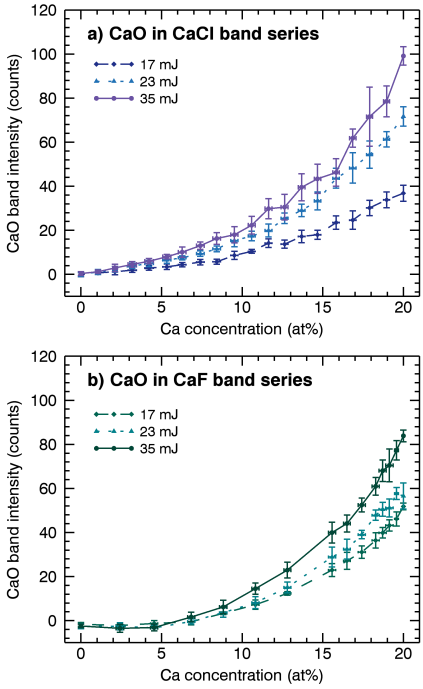

Figure 4: CaO band intensity in the measurements of a) the CaCl band series and b) the CaF band series at different laser energies. The uncertainties represent the standard deviation of the 10 calculated values per sample. No normalization was applied.

contrast, the CaCl band has three distinct maxima, but does not display any comb-like peaks and is generally less intense. The distinct band profiles of these bands do not change noticeably in between the samples used for this study.

CaO emission. The intensity values of the CaO bands that overlap with the bands of CaCl and CaF can be seen in Fig. 4 for the measurements of the samples of the CaCl band series and the CaF band series at different laser energies. For both series, the CaO band intensity quickly decreases towards lower Ca concentrations and higher concentrations of Cl and F. Since

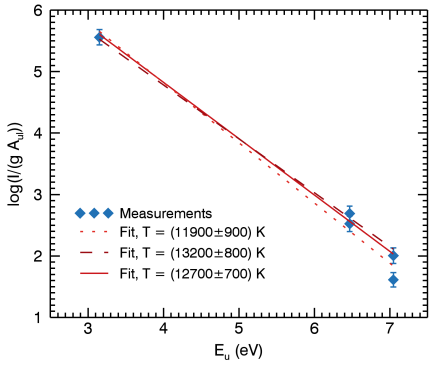

Figure 5: Boltzmann plot to calculate the plasma temperature based on the intensities of five Ca(II) lines. The intensities are taken from the measurements of the $CaCO_3$ sample at a laser energy of 23 mJ/pulse. The uncertainties represent the standard deviation of the 10 calculated values per sample. The solid line is the average of the fits obtained from all 10 spectra, while the two dashed lines are the fits that correspond to the lowest and highest temperatures as obtained from individual spectra.

the O(I) emission does not change significantly for the different samples, a linear relationship between the Ca concentration and the CaO emission would be expected if there was no additional influence on the formation of CaO molecules. The nonlinear relationship that is observed instead could indicate that the formation of CaCl and CaF molecules is favored over the formation of CaO molecules, so that CaO molecules are only formed once no more CaCl or CaF molecules can be formed. For this reason, it is assumed in the following that the formation of CaO is not relevant for the formation of CaCl and CaF.

Electron density and temperature. The electron density and the temperature are important plasma parameters that can be used to estimate the influence of matrix effects on the measurements (Aguilera et al., 2009; Hahn and

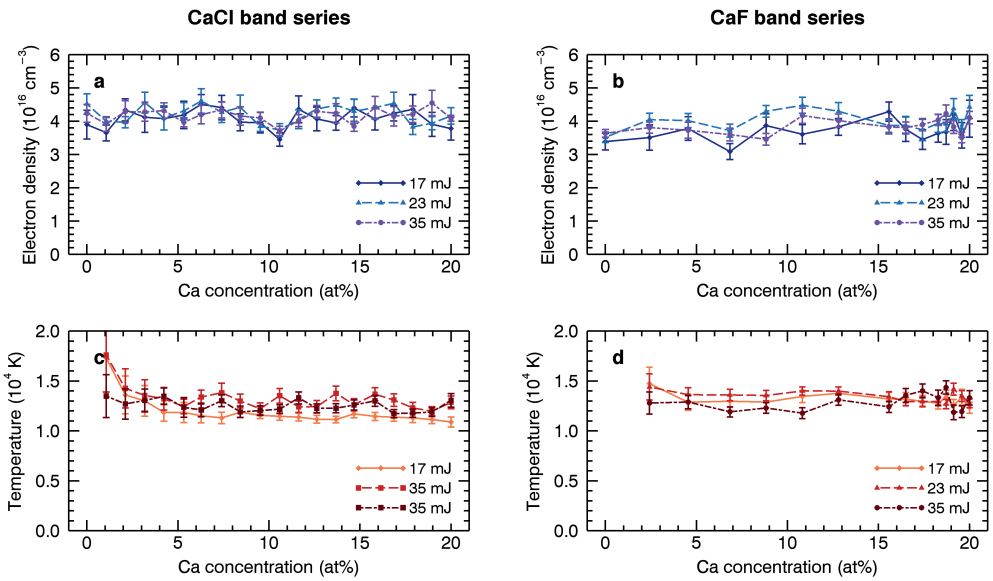

Figure 6: Electron densities for (a) the CaCl band series and (b) the CaF band series as well as temperatures for (c) the CaCl band series and (d) the CaF band series. The values of the electron densities and the temperatures do not change significantly for the three laser energies. The temperature was calculated from Ca(II) lines, so that no temperature could be calculated for the samples without Ca. The uncertainties were calculated from the standard deviation of the 10 measurements per sample in the case of the electron density and from the Boltzmann plot in the case of the temperature.

Omenetto, 2012). The temperature can be calculated from Boltzmann plots, and the electron density can be calculated from the Stark broadening of spectral lines. This broadening is especially strong for the H_α line at 656.3 nm (Fig. 2), so that it is well-suited for the calculation of the electron density (El Sherbini et al., 2006) and has therefore been used in this study. While it has been argued that the H_β line at 486.1 nm is an even better choice (Parigger et al., 2018), it has a very low signal-to-noise ratio in our spectra, making it less suitable for analysis. The electron density n_e was therefore calculated

from the broadening of the H_α line, using the relation (Gigosos et al., 2003)

$$\mathrm{FWHA} = 0.549\,\mathrm{nm} \times \left(\frac{n_e}{10^{17}\,\mathrm{cm}^{-3}}\right)^{0.67965}, \quad (1)$$

where FWHA is the full width at half area of the H_α line. Since a Lorentzian profile was used to fit the line, the FWHA is equal to the full width at half maximum (FWHM).

The temperature has been calculated from Boltzmann plots using the Ca(II) lines at 315.9 nm, 317.9 nm, 370.6 nm, 373.7 nm, and 849.8 nm. These Ca(II) lines were chosen because they are not or only minimally self-absorbed and because they have strong intensities even at low Ca concentrations. Ionic lines were chosen because temperatures calculated from ionic lines are consistently higher than temperatures calculated from neutral lines due to their spatial alignment with high-temperature plasma regions (Aragón and Aguilera, 2008). Fig. 5 shows an example of a Boltzmann plot for the $CaCO_3$ sample, where the uncertainties represent the standard deviation of the intensity values of the individual spectra. For each measured spectrum, a Boltzmann plot was made and a temperature was calculated from the slope of the linear fit. In Fig. 5, the average fit and the fits that correspond to the lowest and the highest calculated temperature are shown to demonstrate the low variability of the measurements.

The values of the electron density and of the temperature are shown in Fig. 6 for all samples and all laser energies. The uncertainties were calculated from the standard deviation of the 10 measurements per sample in the case of the electron density and from the Boltzmann plot in the case of the temperature, as shown in Fig. 5. The electron density stays nearly constant between the various samples of the CaCl and CaF band series, and it is also

not affected by the variation of the laser energy, yielding the same value for 17 mJ/pulse, 23 mJ/pulse, and 35 mJ/pulse. The average electron density of all measurements is about $(4.0 \pm 0.3) \times 10^{16}\,\mathrm{cm}^{-3}$. A similar behavior can be observed for the temperature. For a laser energy of 17 mJ/pulse, the temperature in the CaCl band series decreases slightly, but for most measurements and especially for the higher laser energies it stays close to the average of about $(1.3 \pm 0.1) \times 10^{4}\,\mathrm{K}$. While initially surprising, the observation that neither electron densities nor temperatures are strongly affected by the variation of the laser energy agrees well with previous studies on the influence of the laser energy on these parameters (Yalçin et al., 1999). The results indicate that higher laser energies mostly result in a higher ablation rate. The higher amount of ablated material could then lead to a stronger expansion of the plasma plume until pressure equilibrium is established. At the point of pressure equilibrium, the plasma would be larger in size for higher laser energies, but the particle number densities would still be similar to those at lower laser energies. Likewise, the hot plasma regions could mostly increase in size instead of increasing in temperature. This explanation seems likely, since a dependence of the plasma size on the laser energy has already been observed (Harilal et al., 2015).

The long time gate of 10 µs additionally affects the calculations of the electron density and the temperature. Because the plasma cools over time, electron densities and temperatures are more accurate if they are calculated from measurements with short time gates (50–200 ns). Still, the values that are calculated here can be used as first estimates of the plasma parameters. Since they do not change significantly in between samples, it can be assumed

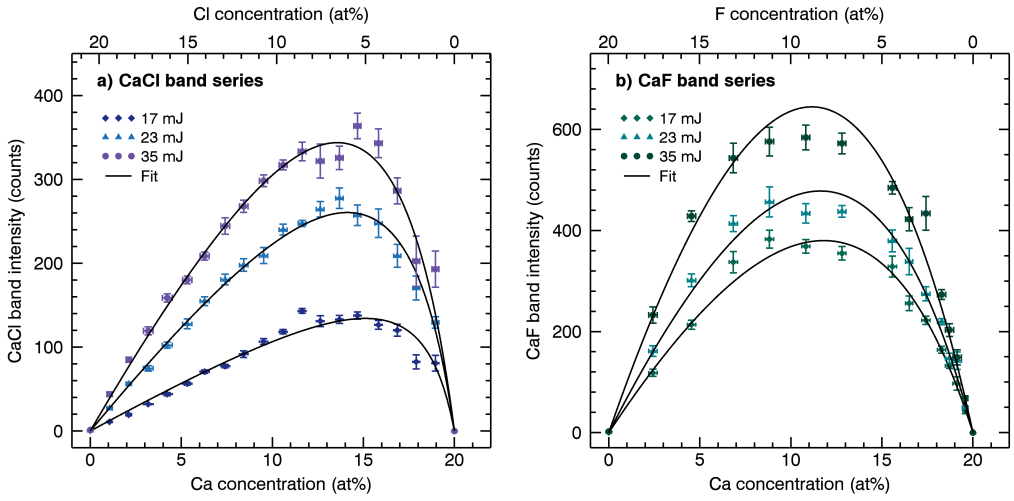

Figure 7: Integrated intensities of a) the CaCl band in the CaCl band series and b) the CaF band in the CaF band series at different laser energies and in dependence of the reactant concentrations. The fit curves are based on Eq. 9 and follow the measured values closely. Uncertainties are calculated from the standard deviations of the 10 measurements per sample. No normalization was applied.

that the conditions in the plasma are similar for all measurements. Therefore, the differences in the intensities measured from the spectra are mostly governed by changes in the sample composition, not by changes in the plasma parameters.

3.2. CaCl and CaF emission in mixed samples (A)

Fig. 7a shows the integrated intensity of the CaCl band for all samples of the CaCl band series in dependence of the Ca concentration and for all three laser energies, with uncertainties calculated from the standard deviation of the measurements. The resulting curves are asymmetrical and skewed towards higher Ca concentrations. This is in contrast to the equivalent curves

in the case of CaF, which can be seen in Fig. 7b for the samples of the CaF band series. For CaF, the curves are nearly symmetrical, and are only slightly skewed towards higher Ca concentrations. Given that the reaction rates for the basic reactions $Ca + Cl \longrightarrow CaCl$ and $Ca + F \longrightarrow CaF$ are equally dependent on the concentrations of both reactants, the observed asymmetry must be related to additional reactions in the plasma that influence the CaCl and CaF concentration. In a previous study, the asymmetry of the CaCl band intensity was mostly attributed to the formation of $CaCl_2$ in the plasma (Vogt et al., 2018). Given that CaF_2 has a higher bond dissociation energy than $CaCl_2$ (5.7±0.4 eV vs. 4.5±0.4 eV, deB. Darwent, 1970) and should therefore be more stable at high temperatures, it was not expected that the asymmetry is less pronounced for CaF.

The influence of CaO formation on these results was minimal. The intensity of the CaO bands decreased quickly towards samples with lower Ca concentrations for both test series, suggesting that CaO formation is less favored than both CaCl formation and CaF formation.

Fit model. The fit shown in Fig. 7 is based on the theoretical intensity of the molecular A-X band, which depends on the chemical processes that are involved. CaCl and CaF are heteronuclear diatomic molecules AB, where A is Ca and B is either Cl or F. The chemical processes are then assumed to be described by the following reactions, based on a similar derivation by

Ogryzlo et al. (1984):

$$\mathrm{A + B \xrightarrow{k_1} AB^*} \tag{2a}$$

$$\mathrm{AB^* \xrightarrow{k_2} A + B} \tag{2b}$$

$$\mathrm{AB^* + B + M \xrightarrow{k_3} AB_2 + M^*} \tag{2c}$$

$$\mathrm{AB^* + M \xrightarrow{k_4} AB + M^*} \tag{2d}$$

$$\mathrm{AB^* + M \xrightarrow{\gamma k_4} AB(A) + M^*} \tag{2e}$$

$$\mathrm{AB(A) + M \xrightarrow{k_5} AB(X) + M^*} \tag{2f}$$

$$\mathrm{AB(A) \xrightarrow{k_6} AB(X) + h\nu} \tag{2g}$$

Reactants A and B recombine to an excited precursor AB^* of the diatomic molecule AB (1a), which can easily dissociate (1b). It can also recombine with a B atom to form AB_2 via a three-body reaction with B and another plasma species M (1c), or recombine to a more stable energy state via collision (1d). A fraction γ will recombine to the $A^2\Pi$ state, indicated here as AB(A) (1e). The backward direction where AB(A) is energized by collision is assumed to be negligible here. Instead it is assumed that AB(A) quickly relaxes to the ground state $X^2\Sigma^+$, indicated here as AB(X), either by collision (1f) or by emitting a photon (1g). The constants above the arrows in (1a–1g) are the rate constants of the reactions. The rate of the radiative transition from the $A^2\Pi$ state to the $X^2\Sigma^+$ state is given by

$$\frac{d[AB(X)]}{dt} = \frac{dn_{h\nu}}{dt} = k_6[AB(A)]\,, \tag{3}$$

where square brackets indicate the number densities of chemical species, and $n_{h\nu}$ is the number density of emitted photons. The intensity of the A-X band

is then proportional to the transition rate of the emission:

$$I_{\text{A-X}} = \frac{h\nu}{4\pi} V k_6 [AB(A)]\,, \tag{4}$$

with the volume of the plasma V and the photon energy $h\nu$ (neglecting the spectral width of the transition). Using the steady-state approximation for AB* and AB(A), their concentrations can be written as:

$$[AB^*] = \frac{k_1[A][B]}{k_2 + k_3[B][M] + k_4[M]} \tag{5}$$

$$[AB(A)] = \frac{\gamma k_4[M]}{k_5[M] + k_6}[AB^*] \tag{6}$$

Since the exact values for the various parameters in Eq. 4–6 are not known and cannot be measured directly, the equations need to be simplified. The first step is to exchange the concentrations [A] and [B] in the plasma for the molar fractions χ_A and χ_B in the sample:

$$[A] = n_{\text{tot}}\chi_A \tag{7}$$

$$[B] = n_{\text{tot}}\chi_B \tag{8}$$

Here n_{tot} is the total number density of atoms in the plasma that were ablated from the sample surface. The assumption here is that nearly stoichiometric ablation is given and that the plasma is relatively uniform. Finally, by grouping the parameters together and by introducing a parameter F for the detection efficiency of the experimental setup (in counts/photon) as well as a parameter Δt for the integration time, the intensity (in counts) can be

written as:

$$I_{\text{A-X}} = \zeta \frac{\chi_A \chi_B}{(1 + \eta \chi_B)} \tag{9}$$

$$\zeta = F \Delta t \, n_{\text{tot}}^2 \frac{k_6 k_1 \gamma k_4 [M]}{(k_5 [M] + k_6)(k_2 + k_4 [M])} \tag{10}$$

$$\eta = n_{\text{tot}} \frac{k_3 [M]}{k_2 + k_4 [M]} \tag{11}$$

The parameter ζ is given in counts of the spectrometer, while η is dimensionless. Since the temperature and the electron density are similar for all measurements (Fig. 6), the rate constants, n_{tot}, and $[M]$ should stay roughly constant for measurements of all samples within a test series at a given laser energy. The relative rate of AB_2 formation in comparison to dissociation and relaxation described by η in Eq. 11 defines how strongly $I_{\text{A-X}}$ is affected by a high concentration χ_B of reactant B. In the special case where both reactants are correlated (e.g. in mixtures containing $CaCl_2$), the intensity of the molecular emission is proportional to the *square* of the analyte concentration (the analyte being one of the reactants) if $\eta \chi_B$ is small. A linear relation between the intensity of the molecular emission and the analyte concentration is only possible if $\eta \chi_B \gg 1$. In that case, the slope m is $m = \zeta / \eta$. Previous measurements of $CaCl_2$ mixtures confirm this, because a quadratic relation was observed at low Cl concentrations and a more linear relation at higher Cl concentrations (Vogt et al., 2018).

Eq. 9 was used to fit the molecular band intensities in Fig. 7. The intensities of both molecular bands can be described accurately for all three laser energies at which they were measured. The fit parameters are listed in Table 2. The results for ζ are similar for the two test series, indicating that the rate constants as well as the concentrations $[M]$ in Eq. 10 are also

Table 2: Fit parameters for the calculation of the band intensity of CaCl and CaF in the CaCl band series and in the CaF band series for all three laser energies.

	CaCl band series		CaF band series	
Laser energy (mJ/pulse)	ζ (counts)	η	ζ (counts)	η
17	$(5.6 \pm 1.1) \times 10^4$	43 ± 10	$(5.7 \pm 0.2) \times 10^4$	5.4 ± 0.6
23	$(7.5 \pm 0.4) \times 10^4$	24 ± 2	$(6.8 \pm 0.3) \times 10^4$	4.7 ± 0.8
35	$(8.3 \pm 0.6) \times 10^4$	17 ± 2	$(8.2 \pm 0.4) \times 10^4$	2.9 ± 0.7

of similar magnitudes. The values of ζ increase for increasing laser energies, which can be explained by the dependence on the total number density n_{tot}. The main difference between the CaCl band series and the CaF band series can be found in η, which is higher in the CaCl band series, indicating that the reaction from $CaCl^*$ to $CaCl_2$ happens at a relatively higher rate than the reaction from CaF^* to CaF_2. The intensity of the CaF band is then only slightly reduced by the $\eta\chi_{\mathrm{F}}$ term in Eq. 9 at high concentrations of F, leading to higher intensities than those of the CaCl band. For increasing laser energies, η decreases in both series. Since the plasma temperature does not change significantly (Fig. 6), the effect could be related to changes in the plasma geometry, which could affect the effective rate constants k_2, k_3, and k_4. The plasma volume has been reported to increase for higher laser energies (Harilal et al., 2015). It is therefore possible that the colder plasma regions, where reactions to $CaCl_2$ and CaF_2 are stable, become smaller relative to the hotter regions as the laser energy is increased. This could effectively reduce the rate constant k_3 and therefore also η.

If a calibration for the Ca concentration is available, Eq. 9 can be used to calculate the concentrations of Cl and F. In the measurements of the

CaCl band series and the CaF band series, the intensity of the Ca(II) line at 373.7 nm is proportional to the Ca concentration in the sample, so that $\chi_A = I_A/m$, where χ_A is the molar fraction of Ca in the sample, I_A is the intensity of the Ca(II) line, and m is the slope of the calibration curve. Then Eq. 9 can be solved for χ_B:

$$\chi_B = \frac{I_{\text{A-X}}}{\zeta I_A/m - \eta I_{\text{A-X}}} \,. \tag{12}$$

Using this equation, the concentrations of Cl in the CaCl band series and of F in the CaF band series were calculated from the ten measurements per sample that were made with a laser energy of 23 mJ/pulse, using the corresponding fit parameters from Table 2. The results can be seen in Fig. 8, where the dotted lines indicate the expected values. At low concentrations of Cl and F, the calculated values are close to the expected values and have a low uncertainty, though the uncertainties for samples of the CaCl band series are consistently higher than the ones for samples of the CaF band series. At high Cl and F concentrations, the calculated concentrations begin to deviate from the true concentrations and the uncertainties increase strongly. The concentration of Cl in the CaCl band series can be calculated correctly up to about 8 at%, while the concentration of F in the CaF band series can be calculated correctly up to about 11 at%. The lower uncertainty of the values in the CaF band series is due to the lower value of η, which reduces the influence of the less accurate second term in the denominator of Eq. 12. Correspondingly, the values are more accurate for high Ca concentrations, because those lead to a high value of the first term in the denominator of Eq. 12. For these two specific test series, in which the Ca concentrations are especially high at low Cl and F concentrations, this leads to highly accurate

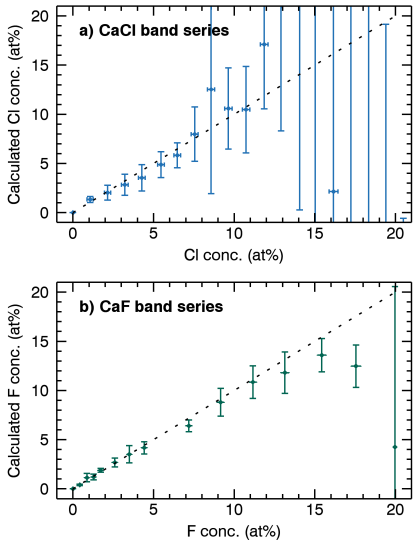

Figure 8: a) Calculated Cl concentration for the CaCl band series. b) Calculated F concentration for the CaF band series. The intensity values were taken from the measurements with a laser energy of 23 mJ/pulse. No normalization was applied. The uncertainties represent the standard deviation of the 10 calculated values per sample.

calculations of the lower Cl and F concentrations. The lowest obtained Cl concentration is (1.3 ± 0.3) at% for the sample with an expected Cl concentration of (1.1 ± 0.2) at% (about 1.8 wt%). The lowest obtained F concentration is (0.40 ± 0.08) at% for the sample with an expected F concentration of (0.42 ± 0.09) at% (about 0.4 wt%).

3.3. Influence of initial bonds (B)

The spectra of the four samples that were investigated for this experiment are shown in Fig. 9 for a laser energy of 23 mJ/pulse. Measurements at 35 mJ/pulse have been done as well and show the same general behavior. An important observation is that the molecular emissions of CaCl and CaF

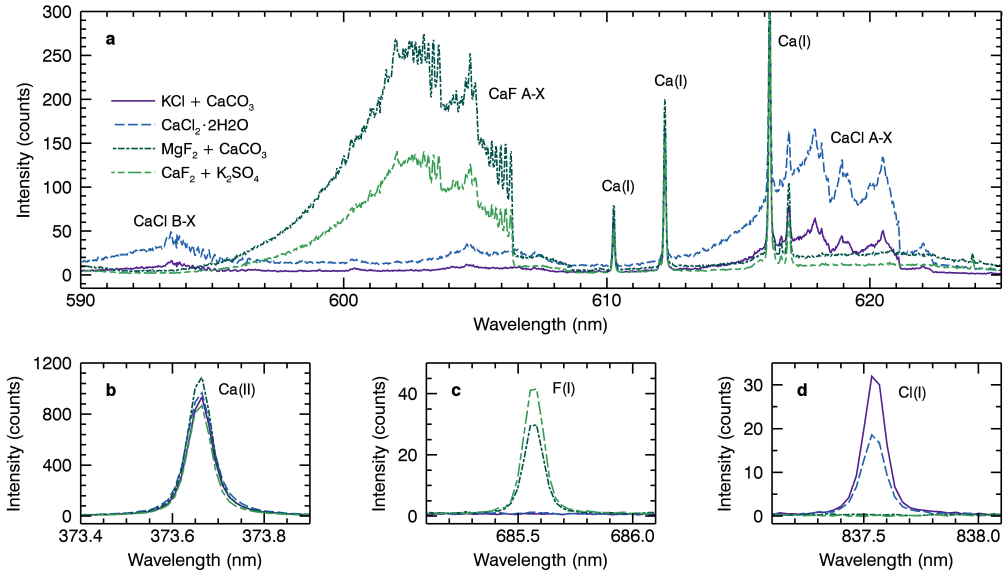

Figure 9: Spectra of samples containing Ca and Cl or Ca and F, either bonded together or from different substances. The laser energy for these measurements was 23 mJ/pulse. (a) The CaCl band is stronger for the sample where Ca and Cl are bound as $CaCl_2$, while the CaF band is weaker for the sample containing CaF_2. (b) The Ca(II) line at 373.6 nm is slightly more intense for the samples with stronger molecular emissions. (c) The F(I) line is weaker for the sample with the stronger CaF emission. (d) The Cl(I) line is weaker for the sample with the stronger CaCl emission.

are affected in opposite ways by the presence of $CaCl_2$ bonds and CaF_2 bonds in the sample. The intensity of the CaCl band is 2.8 times higher for the sample with $CaCl_2$ bonds than it is for the sample where Ca and Cl are not bonded with each other. By contrast, the intensity of the CaF band is 1.9 times lower for the sample containing CaF_2 bonds than it is for the sample without CaF_2 bonds. This behavior of the molecular bands does not correlate with the emission line intensities of the reactants. The intensities of the Ca lines increase slightly for the samples that also have strong band intensities

($CaCl_2 \cdot 2\,H_2O$ and $MgF_2 + CaCO_3$, Fig. 9b). However, the intensities of the halogenic reactants (Cl(I) and F(I), respectively) are significantly lower for these samples than they are for the samples with a lower band intensity (Fig. 9c and d). The actual reactant concentrations are almost equal in each pair of samples and have an uncertainty of less than 0.65 at%, so that the changes in the signal intensities should not be related to differences in the elemental concentrations in the samples. Likewise, the emission line intensities of Ca(II) and F(I) or Cl(I) should be correlated if their changes were caused by differences in the hardness of the sample or in the laser coupling efficiency. As this is not the case, these matrix effects cannot be the dominant factors in the observed intensity changes.

The most likely explanation for the reduced intensity of the Cl(I) line in the $CaCl_2 \cdot 2\,H_2O$ sample and for the reduced intensity of the F(I) line in the $MgF_2 + CaCO_3$ sample is that they are related to the increased formation of CaCl and CaF molecules in these samples, respectively. As the relative difference between the CaCl band intensities is higher than the one between the CaF band intensities, it is reasonable that the reduction of the Cl(I) line intensity is also stronger than that of the F(I) line intensity, as seen in Fig. 9c and d. These results demonstrate that the formation of molecules in the laser-induced plasma is itself a relevant matrix effect that is too strong to be neglected.

The expected increase of the band intensities in spectra of samples in which the two reactants are already bonded could only be observed for CaCl, but the opposite was true for CaF, where the band intensity was lower for the sample with CaF_2 bonds. While the cause of the observed differences is

unknown, the large differences of the band intensities for samples with equal reactant concentrations are a clear sign of the influence of matrix effects on the formation of molecules in the plasma.

3.4. Influence of competing molecule formation (C)

Fig. 10 shows the intensities of the CaCl and CaF emission in the two test series in which the concentration of one reactant is increased while that of the other stays at roughly the same value. In Fig. 10a and b, the Cl concentration is varied. Even though the CaCl band is clearly increasing in intensity, the CaF band is not significantly affected. In the sample with the highest molar fraction of Cl, there is three times as much Cl in the sample as F, but the CaF band intensity is still close to its average intensity. This is a clear indication that the CaF emission band is not strongly affected by the formation of CaCl in the plasma.

The increase of the CaCl band in Fig. 10a can be fitted with Eq. 9. However, the parameters from Table 2 for the CaCl band do not fit well in this case. They are found to be smaller, with $\zeta = (3.6 \pm 0.3) \times 10^4$ counts and $\eta = 5.7 \pm 2.2$. A smaller η means that the rate of reactions to $CaCl_2$ is reduced, since the other parameters in η mostly depend on the number densities and the temperature, which did not change in comparison to experiment A. While it is possible that the plasma dimensions for these samples are unfavorable for reactions to $CaCl_2$, it is more likely that the parameters are actually similar to those from Table 2, but that the concentration of available Ca in the plasma is changed due to the presence of CaF. This would lead to a false calculation of the fit parameters, which would be smaller in this case.

In contrast to the CaF band in the previous case, the CaCl band in

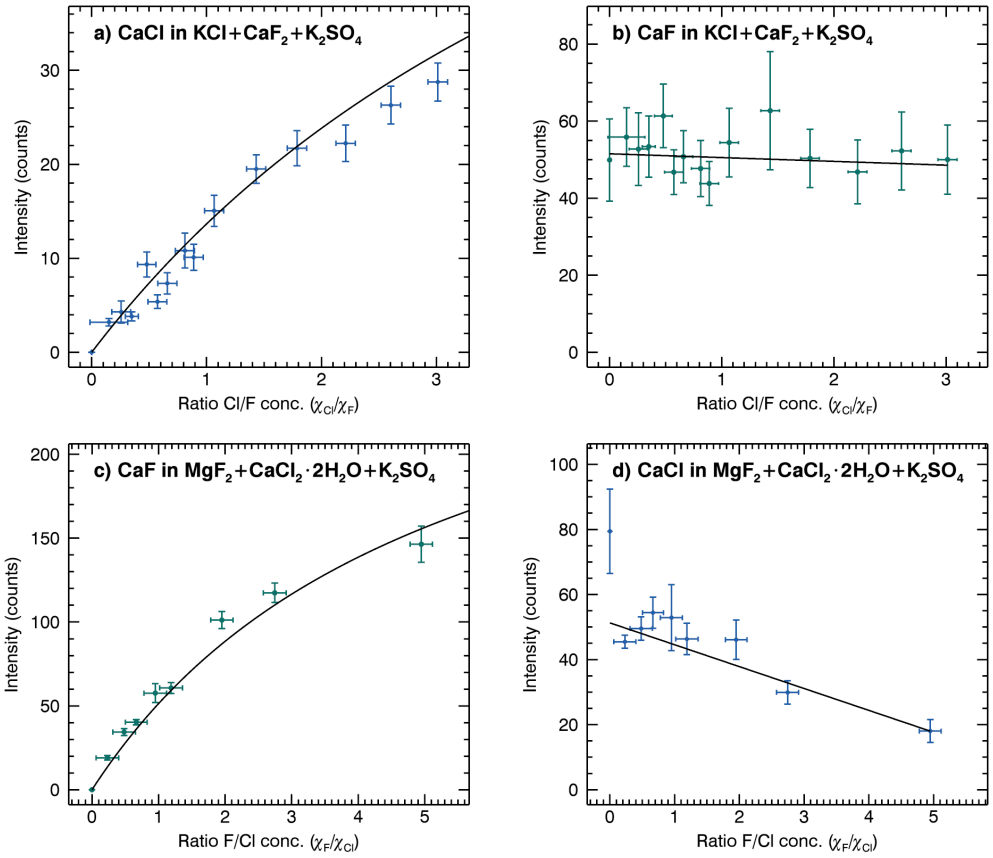

Figure 10: Intensities of the CaCl band and the CaF band in the samples of the robustness series. Top row: The molar fractions of Ca and F are constant while the Cl fraction is varied to up to 3 times the F fraction. Bottom row: The molar fractions of Ca and Cl are constant, while F is varied between 0 and 5 times the Cl fraction. For constant Ca and F concentrations, the CaF band stays at the same intensity despite the increasing Cl concentration (b). By contrast, the CaCl band intensity significantly decreases as the F concentration increases even though the concentrations of Ca and Cl stay constant (d). No normalization was applied to the intensities in (a). The intensities in (b) and (d) are normalized with the Ca(II) line at 373.7 nm, the intensities in (c) are normalized with Mg(II) (293.6 nm).

Fig. 10d is strongly affected by the additional formation of CaF in the plasma. There is a clear decrease in the intensity as the F concentration increases. In the sample with the highest F concentration, the CaCl band is approximately three times weaker than it is in samples with low F concentrations. This again supports the idea that CaF formation is favored over CaCl formation. The fit for the CaF band is interesting because in this case, the two fit parameters are higher than they are in Table 2 with $\zeta = (1.4 \pm 0.1) \times 10^5$ counts and $\eta = 6.4 \pm 2.2$. The value of ζ is twice as high as the value that was found for the CaF band series at 23 mJ/pulse. However, the plasma parameters are comparable to those of the previous experiments, so that none of the parameters in ζ should significantly change. Since both CaCl and CaF molecules are formed, it would even be expected that the rate of CaF formation would be slightly smaller than in experiment A. Therefore it seems likely that the increased intensity of CaF is again based on matrix effects during the ablation process, similar to the case observed in experiment B, where the band intensities changed in dependence on the bonds in the sample.

The intensities of the CaF band in Fig. 10b and the CaCl band in Fig. 10d have been normalized with the Ca(II) line intensity at 373.7 nm because they showed a high variation. This variation was strongly correlated with that of the Ca lines, which indicates that the concentrations of the relevant substances in the mixtures (CaF_2 and $CaCl_2$, respectively) varied a lot. The reason for this variation is the ternary mixing process that was required. It is more challenging to make homogeneous samples from ternary mixtures, as the likelihood of three components being equally distributed in the sample is lower than it is for two components. We tried to compensate for this

by increasing the number of measurements per sample from 10 to 15, but in some cases the average and median intensities were nevertheless different from their expected values. This mostly affects the molecular bands where both reactants come from the same component in the mixture, as in this case both concentrations increase or decrease at the same time, while in the other case a decrease in the concentration of one reactant can often be compensated by an increase of the concentration of the other reactant.

4. Discussion

The influences of varying reactant concentrations (experiment A), changes in the initial bonds (experiment B), and competing molecule formation (experiment C) on the band intensities of CaCl and CaF were investigated. The appearance of the molecular bands was not noticeably affected in either of these experiments, as the fit that was made to calculate the band intensities matched their profiles very well for all samples. Since the appearance of a molecular band can change depending on the temperature of the plasma (Herzberg, 1950), this indicates that the molecules were formed in regions with similar temperatures. This is in line with plasma simulations, which usually find that the formation of molecules happens within a comparatively low and narrow temperature range, e.g. 3000–7000 K for CaCl (Shabanov and Gornushkin, 2016).

In experiment A, the molecular bands of CaCl and CaF disappear if either of the reactants is missing. In between, the band intensity quickly rises, but in both cases an asymmetry can be observed, so that the maximum band intensities are shifted towards higher Ca concentrations. This effect is

significantly stronger in the case of CaCl than it is for CaF and has already been observed in our last study on CaCl, where it was attributed to reactions to $CaCl_2$ (Vogt et al., 2018). We introduced a new theoretical description from a model of chemical reactions, approximating the molecule formation as a steady-state process. This approximation should be justified for laser-induced plasmas in partial local thermal equilibrium, since the three-body collisions involved in the chemical processes happen within the same time scale as collisional ionization and three-body recombination. The result is an effective way to describe the intensities of CaCl and CaF bands with only two fit parameters (Eq. 9). Despite the strong differences that could be observed between the intensities of the CaCl band series and the CaF band series, the fit function was able to describe both cases accurately for measurements at three different laser energies. The simplicity of the fit is a big advantage that might also enable the integration of molecular analysis into the standard processes that are used to analyze Martian LIBS spectra. While the numerical fit routine in our last study on CaCl was able to produce very good time-resolved results at the cost of a high complexity (Vogt et al., 2018), the fit function of the present study is the most simple description of molecular band intensities that seems possible without sacrificing accuracy. This approach seems more suitable for quantitative analysis in the context of planetary exploration, where time-resolved LIBS spectra are usually not available.

In order to use the model described here to calculate unknown elemental concentrations, the two parameters ζ and η need to be determined for the specific LIBS instrument that is used to measure the spectra, and a cali-

bration curve for the Ca concentration needs to be available. Equation 12 can then be used to calculate the concentration of Cl or F. The calculated concentrations are more accurate for low values of η and for samples with high Ca concentrations, so that the most accurate values in the two investigated series were actually obtained for the samples with the lowest Cl and F concentrations above zero: (1.3 ± 0.3) at% for Cl and (0.40 ± 0.08) at% for F. The Cl concentration is less accurate due to the higher value of η for the CaCl band series. For Martian LIBS spectra, the laser irradiance may vary between measurements, so that the dependence of the parameters on the laser irradiance (Table 2) needs to be considered. As the pulse energy increases, ζ increases and η decreases for both CaCl and CaF. Ideally, the two parameters are determined for several values of the laser irradiance. However, the asymmetric shape of the curves in Fig. 7, which is determined by η, is not strongly affected by the change of the pulse energy, despite the variations in the best-fitting parameter values. Therefore an approximate value for η might be sufficient in many situations. Then the only important influence of the laser irradiance is on ζ, which is a scaling factor that can likely be accounted for by normalization. This is promising for the application of the model to ChemCam and SuperCam data, where the irradiance changes with the distance to the target.

In experiment B, molecular formation following fragmentation was investigated. This is an alternative to the formation of molecules via chemical reactions in the plasma. Fragmentation may occur during the ablation process (Doucet et al., 2008). In this case, polyatomic fragments are ejected from the sample surface, which then thermally dissociate in the plasma. This ther-

mal dissociation may lead to the formation of CaCl and CaF molecules, but only if bonds between these elements were already present in the sample. For this reason, molecular emissions from samples with and without native bonds of $CaCl_2$ and CaF_2 were compared. While significant differences in the band intensities were indeed observed, the effect was inverted for CaCl and CaF: the CaCl band intensity strongly increased if $CaCl_2$ bonds were present, but the CaF band intensity strongly decreased in an equivalent comparison. If fragmentation is the dominant effect behind these changes, then the differences for CaCl and CaF might be explained by differences in the dissociation energies of their original bonds. The energy required for the dissociation $CaF_2 \longrightarrow CaF + F$ is 5.7 ± 0.4 eV, while that of $CaCl_2 \longrightarrow CaCl + Cl$ is only 4.5 ± 0.4 eV (deB. Darwent, 1970). Therefore it is possible that less CaF_2 fragments dissociate before they move out of the high-temperature plasma regions. However, the MgF_2 bonds in the comparison sample for the CaF band have a slightly higher dissociation energy than CaF_2 with 5.9 ± 0.4 eV (deB. Darwent, 1970), which should then also reduce the CaF band intensity in the comparison sample. It is therefore not clear if fragmentation is the dominant effect that influences the band intensities here, or if other matrix effects are also relevant. However, even though we originally expected that the band intensities would increase for all samples with native bonds between the reactants, the results clearly demonstrate a large influence of the native bonds on the band intensities. For the reaction model developed in experiment A, this could mean that different parameters have to be used if native bonds of the reactants are present in the sample. In mixed cases where only a fraction of the reactants are bound together in the sample, a superposition of two

reaction models would have to be used that is weighted in correspondence to the expected ratios in the sample. To distinguish between these different cases, it is important to have additional information about the sample, for example from a multivariate analysis of the LIBS spectrum and from context images. However, Martian targets in which these native bonds might pose a challenge are limited: the only minerals with native bonds of Ca and Cl are sinjarite ($CaCl_2 \cdot 2\,H_2O$) and antarcticite ($CaCl_2 \cdot 6\,H_2O$), while fluorite (CaF_2) is the only mineral with native bonds of Ca and F.

The results of experiment C show that the molecular emission of CaF is less affected by the competing formation of CaCl than the other way around. The intensity of the CaCl emission strongly decreased for increasing amounts of fluorine in the sample, while the CaF band was not significantly affected by an increasing chlorine concentration. This suggests that CaF formation is favored over CaCl formation and that CaF is generally more stable than CaCl. The low η values of the CaF band intensity fits in experiment A and the higher dissociation energy of CaF in comparison to that of CaCl (5.7 ± 0.4 eV vs. 4.4 ± 0.4 eV, deB. Darwent, 1970) support this, since the low η value indicates a low rate of CaF_2 formation and a higher dissociation energy indicates a more stable bond. There is a potential unaccounted influence of fragmentation in the results of experiment C, however, as it was necessary to use samples containing $CaCl_2$ and CaF_2 bonds in this experiment in order to avoid the preparation of complex and error-prone quaternary mixtures. The measurements also showed a high variation and had to be normalized, which was attributed to the uncertainties in the mixing process. For future studies on this topic, it might be advantageous to avoid a ternary mixing process

by preparing binary mixtures that are then mixed in a binary process again, similar to the mixtures prepared for experiment A.

The observation that electron densities and temperatures did not change significantly for higher laser energies requires further investigation. It is possible that the excess energy leads to a higher ablation rate, but not to a stronger heating of the plasma plume. The higher ablation rate could then result in a larger plasma volume in which the particle number densities are similar as in the plasma measured at a lower laser energy. The results from previous studies in terrestrial ambient conditions seem to support this explanation (Yalçin et al., 1999; Harilal et al., 2015). The effect could be even more pronounced at the lower Martian atmospheric pressure, in which the plasma plume is less confined. The dependence of the plasma volume and the plasma temperature on the laser energy in Martian ambient conditions will therefore be investigated in a future study with a plasma imaging setup for spatially resolved measurements of the plasma emissions.

5. Conclusion

Molecular bands of CaCl and CaF in the laser-induced plasma were investigated under simulated Martian conditions in order to examine their potential for the quantification of Cl and F on Mars. They are often much more intense than emission lines of Cl and F, but several matrix effects need to be considered in their quantitative analysis. The most important factor is the dependence of the band intensities on the concentrations of the two components (Ca and Cl or Ca and F, respectively). A fit function (Eq. 9) to describe this dependence was derived from rate equations under the assump-

tion of a steady state. It only requires two parameters to accurately describe the intensities of both the CaCl band and the CaF band, and it can be used in an equivalent manner as a usual calibration curve. If a calibration for the Ca concentration is available, the model can be used to calculate the Cl concentration from the CaCl band intensity and the F concentration from the CaF band intensity. This provides a theoretical framework for experimental observations that is easier to use than the numerical models that have been suggested before, (e.g. Shabanov and Gornushkin, 2015; Vogt et al., 2018). The lowest detected concentrations in this study were 1.8 wt% Cl and 0.4 wt% F, which could likely be reduced even further since the measurements were not close to the detection limit.

In addition to their concentrations, the initial bonds of Ca and Cl or Ca and F were found to strongly influence the band intensities. A potential explanation for this is fragmentation, which can produce CaCl or CaF molecules as fragments of the original salts $CaCl_2$ and CaF_2 if these are present in the sample. The band intensity of CaCl increased if $CaCl_2$ was present in the original sample matrix, while that of CaF decreased if CaF_2 was present. These differences might be due to different dissociation energies of $CaCl_2$ and CaF_2, but further research is necessary to determine whether other matrix effects contribute to the observed differences as well. Temporally and spatially resolved measurements could help to clarify the role of fragmentation, as emissions by molecules that formed as fragments of the original matrix should occur in earlier stages of the plasma and closer to the sample surface than emissions of molecules formed by chemical reactions. Since the only minerals with bonds between Ca and Cl or Ca and F are

sinjarite, antarcticite, and fluorite, multivariate analysis and context images should make it possible to identify Martian targets in which these bonds might influence the molecular band intensities.

The investigation of the competing formation of CaCl and CaF suggests that CaF formation is more dominant, as the CaF band was not affected by the formation of CaCl, while the CaCl band was strongly affected by the formation of CaF. The effect can therefore be neglected for CaF, especially in comparison to the stronger influence of the initial bonds and potential fragmentation. For CaCl, competing molecular formation can be more relevant. The reduction of the band intensity needs to be considered if both CaCl and CaF bands can be observed, which could be the case for apatites containing both F and Cl anions. It is also possible that only the CaF band can be observed even if a small concentration of Cl is present in the sample as well.

This study was made to support the analysis of LIBS spectra of the Martian surface measured by instruments like ChemCam or SuperCam. While the results are relevant to molecular LIBS in general, they are especially important in the context of Martian exploration. The detection and quantification of Cl and F provides crucial information about the geological and fluvial history of Mars. Analyzing and understanding the matrix effects that can influence the intensities of the strongest signals related to Cl and F is necessary in order to accurately quantify their presence in Martian environments. The application of these results to Martian LIBS data will be an important next step.

References

Aguilera, J.A., Aragón, C., Madurga, V., Manrique, J., 2009. Study of matrix effects in laser induced breakdown spectroscopy on metallic samples using plasma characterization by emission spectroscopy. Spectrochimica Acta - Part B Atomic Spectroscopy 64, 993–8. doi:10.1016/j.sab.2009.07.007.

Alvarez-Llamas, C., Pisonero, J., Bordel, N., 2016. Quantification of fluorine traces in solid samples using CaF molecular emission bands in atmospheric air LIBS. Spectrochimica Acta - Part B Atomic Spectroscopy 123, 157–62. doi:10.1016/j.sab.2016.08.006.

Aragón, C., Aguilera, J.A., 2008. Characterization of laser induced plasmas by optical emission spectroscopy: A review of experiments and methods. Spectrochimica Acta - Part B Atomic Spectroscopy 63, 893–916. doi:10.1016/j.sab.2008.05.010.

Asundi, R.K., 1935. The band systems and structure of CaCl. Proceedings of the Indian Academy of Sciences - Section A 1, 830–40. doi:10.1007/BF03035639.

Beck, P., Fau, A., Meslin, P.Y., Forni, O., Lasue, J., Lewin, E., Cousin, A., Maurice, S., Rapin, W., Gasnault, O., Wiens, R.C., Mangold, N., Sautter, V., Coll, P., Szopa, C., Dequaire, T., Garcia, B., Schwartz, S., 2017. Searching for Carbon on Mars with MSL/ChemCam.

Burt, D.M., Knauth, L.P., 2003. Electrically conducting, Ca-rich brines, rather than water, expected in the Martian subsurface. Journal of Geophysical Research 108. doi:10.1029/2002je001862.

Clark, B.C., Kounaves, S.P., 2016. Evidence for the distribution of perchlorates on Mars. International Journal of Astrobiology 15, 311–8. doi:10.1017/S1473550415000385.

Cremers, D.A., Radziemski, L.J., 2006. Handbook of Laser-induced Breakdown Spectroscopy. John Wiley & Sons, Ltd, Chichester, UK. doi:10.1002/0470093013.

deB. Darwent, B., 1970. Bond dissociation energies in simple molecules. National Bureau of Standards.

Doucet, F.R., Faustino, P.J., Sabsabi, M., Lyon, R.C., 2008. Quantitative molecular analysis with molecular bands emission using laser-induced breakdown spectroscopy and chemometrics, in: Journal of Analytical Atomic Spectrometry, The Royal Society of Chemistry. pp. 694–701. doi:10.1039/b714219f.

El Sherbini, A.M., Hegazy, H., El Sherbini, T.M., 2006. Measurement of electron density utilizing the Hα-line from laser produced plasma in air. Spectrochimica Acta - Part B Atomic Spectroscopy 61, 532–9. doi:10.1016/j.sab.2006.03.014.

Filiberto, J., Gross, J., McCubbin, F.M., 2016. Constraints on the water, chlorine, and fluorine content of the Martian mantle. Meteoritics and Planetary Science 51, 2023–35. doi:10.1111/maps.12624.

Filiberto, J., Treiman, A.H., 2009a. Martian magmas contained abundant chlorine, but little water. Geology 37, 1087–90. doi:10.1130/G30488A.1.

Filiberto, J., Treiman, A.H., 2009b. The effect of chlorine on the liquidus of basalt: First results and implications for basalt genesis on Mars and Earth. Chemical Geology 263, 60–8. doi:10.1016/J.CHEMGEO.2008.08.025.

Filiberto, J., Wood, J., Dasgupta, R., Shimizu, N., Le, L., Treiman, A.H., 2012. Effect of fluorine on near-liquidus phase equilibria of an Fe-Mg rich basalt. Chemical Geology 312-313, 118–26. doi:10.1016/j.chemgeo.2012.04.015.

Forni, O., Gaft, M., Toplis, M.J., Clegg, S.M., Maurice, S., Wiens, R.C., Mangold, N., Gasnault, O., Sautter, V., Le Mouélic, S., Meslin, P.Y., Nachon, M., McInroy, R.E., Ollila, A.M., Cousin, A., Bridges, J.C., Lanza, N.L., Dyar, M.D., 2015. First detection of fluorine on Mars: Implications for Gale Crater's geochemistry. Geophysical Research Letters 42, 1020–8. doi:10.1002/2014GL062742.

Gaft, M., Nagli, L., Eliezer, N., Groisman, Y., Forni, O., 2014. Elemental analysis of halogens using molecular emission by laser-induced breakdown spectroscopy in air. Spectrochimica Acta - Part B Atomic Spectroscopy 98, 39–47. doi:10.1016/j.sab.2014.05.011.

Gasda, P.J., Haldeman, E.B., Wiens, R.C., Rapin, W., Bristow, T.F., Bridges, J.C., Schwenzer, S.P., Clark, B., Herkenhoff, K., Frydenvang, J., Lanza, N.L., Maurice, S., Clegg, S., Delapp, D.M., Sanford, V.L., Bodine, M.R., McInroy, R., 2017. In situ detection of boron by ChemCam on Mars. Geophysical Research Letters 44, 8739–48. doi:10.1002/2017GL074480.

Gasnault, O., Mazoyer, J., Cousin, A., Meslin, P.Y., Lasue, J., Lacour, J.L.,

Ollila, A., Berger, G., Forni, O., Maurice, S., Wiens, R.C., Clegg, S., Blank, J., 2012. Deciphering Sample and Atmospheric Oxygen Contents with ChemCam on Mars, in: 43rd Lunar and Planetary Science Conference, p. 2888.

Gigosos, M.A., González, M.Á., Cardeñoso, V., 2003. Computer simulated Balmer-alpha, -beta and -gamma Stark line profiles for non-equilibrium plasmas diagnostics, in: Spectrochimica Acta - Part B Atomic Spectroscopy, Elsevier. pp. 1489–504. doi:10.1016/S0584-8547(03)00097-1, arXiv:arXiv:1011.1669v3.

Grotzinger, J.P., Crisp, J., Vasavada, A.R., Anderson, R.C., Baker, C.J., Barry, R., Blake, D.F., Conrad, P., Edgett, K.S., Ferdowski, B., Gellert, R., Gilbert, J.B., Golombek, M., Gómez-Elvira, J., Hassler, D.M., Jandura, L., Litvak, M., Mahaffy, P., Maki, J., Meyer, M., Malin, M.C., Mitrofanov, I., Simmonds, J.J., Vaniman, D., Welch, R.V., Wiens, R.C., 2012. Mars Science Laboratory mission and science investigation. Space Science Reviews 170, 5–56. doi:10.1007/s11214-012-9892-2.

Hahn, D.W., Omenetto, N., 2012. Laser-induced breakdown spectroscopy (LIBS), part II: Review of instrumental and methodological approaches to material analysis and applications to different fields. Applied Spectroscopy 66, 347–419. doi:10.1366/11-06574.

Harilal, S.S., Brumfield, B.E., Phillips, M.C., 2015. Lifecycle of laser-produced air sparks. Physics of Plasmas 22, 063301. doi:10.1063/1.4922076.

Harri, A.M., Genzer, M., Kemppinen, O., Kahanpää, H., Gomez-Elvira, J., Rodriguez-Manfredi, J.A., Haberle, R., Polkko, J., Schmidt, W., Savijärvi, H., Kauhanen, J., Atlaskin, E., Richardson, M., Siili, T., Paton, M., de la Torre Juarez, M., Newman, C., Rafkin, S., Lemmon, M.T., Mischna, M., Merikallio, S., Haukka, H., Martin-Torres, J., Zorzano, M.P., Peinado, V., Urqui, R., Lapinette, A., Scodary, A., Mäkinen, T., Vazquez, L., Rennó, N., the REMSMSL Science Team, t.R.S., 2014. Pressure observations by the Curiosity rover: Initial results. Journal of Geophysical Research: Planets 119, 82–92. doi:10.1002/2013JE004423.

Hecht, M.H., Kounaves, S.P., Quinn, R.C., West, S.J., Young, S.M., Ming, D.W., Catling, D.C., Clark, B.C., Boynton, W.V., Hoffman, J., DeFlores, L.P., Gospodinova, K., Kapit, J., Smith, P.H., 2009. Detection of perchlorate and the soluble chemistry of martian soil at the phoenix lander site. Science 325, 64–7. doi:10.1126/science.1172466.

Herzberg, G., 1950. Spectra of Diatomic Molecules. 2nd editio ed., Van Nostrand.

Knight, A.K., Scherbarth, N.L., Cremers, D.A., Ferris, M.J., 2000. Characterization of laser-induced breakdown spectroscopy (LIBS) for application to space exploration. Applied Spectroscopy 54, 331–40. doi:10.1366/0003702001949591.

Le Mouélic, S., Gasnault, O., Herkenhoff, K.E., Bridges, N.T., Langevin, Y., Mangold, N., Maurice, S., Wiens, R.C., Pinet, P., Newsom, H.E., Deen, R.G., Bell, J.F., Johnson, J.R., Rapin, W., Barraclough, B., Blaney, D.L., Deflores, L., Maki, J., Malin, M.C., Pérez, R., Saccoccio, M., 2015. The

ChemCam Remote Micro-Imager at Gale crater: Review of the first year of operations on Mars. Icarus 249, 93–107. doi:10.1016/j.icarus.2014.05.030.

Marks, R.F., Gottscho, R.A., Field, R.W., 1982. The CaO D,d1,3Δ-a3Π System: Sub-Doppler Spectrum, Rotational Analysis, and Deperturbation. Physica Scripta 25, 312–28. doi:10.1088/0031-8949/25/2/010.

Massé, M., Bourgeois, O., Le Mouélic, S., Verpoorter, C., Le Deit, L., Bibring, J.P., 2010. Martian polar and circum-polar sulfate-bearing deposits: Sublimation tills derived from the North Polar Cap. Icarus 209, 434–51. doi:10.1016/j.icarus.2010.04.017.

Maurice, S., Clegg, S.M., Wiens, R.C., Gasnault, O., Rapin, W., Forni, O., Cousin, A., Sautter, V., Mangold, N., Le Deit, L., Nachon, M., Anderson, R.B., Lanza, N.L., Fabre, C., Payré, V., Lasue, J., Meslin, P.Y., Léveillé, R.J., Barraclough, B.L., Beck, P., Bender, S.C., Berger, G., Bridges, J.C., Bridges, N.T., Dromart, G., Dyar, M.D., Francis, R., Frydenvang, J., Gondet, B., Ehlmann, B.L., Herkenhoff, K.E., Johnson, J.R., Langevin, Y., Madsen, M.B., Melikechi, N., Lacour, J.L., Le Mouélic, S., Lewin, E., Newsom, H.E., Ollila, A.M., Pinet, P., Schröder, S., Sirven, J.B., Tokar, R.L., Toplis, M.J., D'Uston, C., Vaniman, D.T., Vasavada, A.R., 2016. ChemCam activities and discoveries during the nominal mission of the Mars Science Laboratory in Gale crater, Mars. doi:10.1039/c5ja00417a.

Maurice, S., Wiens, R.C., Saccoccio, M., Barraclough, B., Gasnault, O., Forni, O., Mangold, N., Baratoux, D., Bender, S., Berger, G., Bernardin, J., Berthé, M., Bridges, N., Blaney, D., Bouyé, M., Caïs, P., Clark, B.,

Clegg, S., Cousin, A., Cremers, D., Cros, A., Deflores, L., Derycke, C., Dingler, B., Dromart, G., Dubois, B., Dupieux, M., Durand, E., D'Uston, L., Fabre, C., Faure, B., Gaboriaud, A., Gharsa, T., Herkenhoff, K., Kan, E., Kirkland, L., Kouach, D., Lacour, J.L., Langevin, Y., Lasue, J., Le Mouélic, S., Lescure, M., Lewin, E., Limonadi, D., Manhès, G., Mauchien, P., McKay, C., Meslin, P.Y., Michel, Y., Miller, E., Newsom, H.E., Orttner, G., Paillet, A., Parès, L., Parot, Y., Pérez, R., Pinet, P., Poitrasson, F., Quertier, B., Sallé, B., Sotin, C., Sautter, V., Séran, H., Simmonds, J.J., Sirven, J.B., Stiglich, R., Striebig, N., Thocaven, J.J., Toplis, M.J., Vaniman, D., 2012. The ChemCam instrument suite on the Mars Science Laboratory (MSL) rover: Science objectives and mast unit description. Space Science Reviews 170, 95–166. doi:10.1007/s11214-012-9912-2.

Meslin, P., Cicutto, L., Forni, O., Drouet, C., Rapin, W., Nachon, M., Cousin, A., Blank, J.G., McCubbin, F.M., Gasnault, O., Newsom, H., Mangold, N., Schröder, S., Sautter, V., Maurice, S., Wiens, R.C., 2016. Calibration of the Fluorine, Chlorine, and Hydrogen Content of Apatites with the ChemCam LIBS Instrument.

Möhlmann, D., Thomsen, K., 2011. Properties of cryobrines on Mars. Icarus 212, 123–30. doi:10.1016/j.icarus.2010.11.025.

Nachon, M., Clegg, S.M., Mangold, N., Schröder, S., Kah, L.C., Dromart, G., Ollila, A., Johnson, J.R., Oehler, D.Z., Bridges, J.C., Le Mouélic, S., Forni, O., Wiens, R.C., Anderson, R.B., Blaney, D.L., Bell, J.F., Clark, B., Cousin, A., Dyar, M.D., Ehlmann, B., Fabre, C., Gasnault, O., Grotzinger, J., Lasue, J., Lewin, E., Léveillé, R., McLennan, S., Maurice, S., Meslin,

P.Y., Rapin, W., Rice, M., Squyres, S.W., Stack, K., Sumner, D.Y., Vaniman, D., Wellington, D., 2014. Calcium sulfate veins characterized by ChemCam/Curiosity at Gale crater, Mars. Journal of Geophysical Research E: Planets 119, 1991–2016. doi:10.1002/2013JE004588.

Ogryzlo, E.A., Shen, Y.Q., Wassell, P.T., 1984. The yield of O2(b1Σg+) in oxygen atom recombination. Journal of Photochemistry 25, 389–98. doi:10.1016/0047-2670(84)87040-9.

Ollila, A.M., Blank, J.G., Wiens, R.C., Lasue, J., Newsom, H.E., Clegg, S.M., Cousin, A., Maurice, S., 2011. Preliminary Results on the Capabilities of the ChemCam Laser-Induced Breakdown Spectroscopy (LIBS) Instrument to Detect Carbon on Mars.

Osterloo, M.M., Anderson, F.S., Hamilton, V.E., Hynek, B.M., 2010. Geologic context of proposed chloride-bearing materials on Mars. Journal of Geophysical Research E: Planets 115, E10012. doi:10.1029/2010JE003613.

Parigger, C., Drake, K., Helstern, C., Gautam, G., 2018. Laboratory Hydrogen-Beta Emission Spectroscopy for Analysis of Astrophysical White Dwarf Spectra. Atoms 6, 36. doi:10.3390/atoms6030036.

Perez, D., Lewis, L.J., 2002. Ablation of Solids under Femtosecond Laser Pulses. Physical Review Letters 89, 255504. doi:10.1103/PhysRevLett.89.255504.

Radzig, A.A., Smirnov, B.M., 1985. Reference Data on Atoms, Molecules, and Ions. volume 31 of *Springer Series in Chemical Physics*. Springer

Berlin Heidelberg, Berlin, Heidelberg. doi:10.1007/978-3-642-82048-9, arXiv:arXiv:1011.1669v3.

Rapin, W., Meslin, P.Y., Maurice, S., Vaniman, D., Nachon, M., Mangold, N., Schröder, S., Gasnault, O., Forni, O., Wiens, R.C., Martínez, G.M., Cousin, A., Sautter, V., Lasue, J., Rampe, E.B., Archer, D., 2016. Hydration state of calcium sulfates in Gale crater, Mars: Identification of bassanite veins. Earth and Planetary Science Letters 452, 197–205. doi:10.1016/j.epsl.2016.07.045.

Schröder, S., Meslin, P.Y., Gasnault, O., Maurice, S., Cousin, A., Wiens, R.C., Rapin, W., Dyar, M.D., Mangold, N., Forni, O., Nachon, M., Clegg, S., Johnson, J.R., Lasue, J., Le Mouélic, S., Ollila, A., Pinet, P., Sautter, V., Vaniman, D., 2015. Hydrogen detection with ChemCam at Gale crater. Icarus 249, 43–61. doi:10.1016/j.icarus.2014.08.029.

Schröder, S., Pavlov, S.G., Rauschenbach, I., Jessberger, E.K., Hübers, H.W., 2013. Detection and identification of salts and frozen salt solutions combining laser-induced breakdown spectroscopy and multivariate analysis methods: A study for future martian exploration. Icarus 223, 61–73. doi:10.1016/j.icarus.2012.11.011.

Schröder, S., Rammelkamp, K., Vogt, D., Gasnault, O., Hübers, H.W., 2019. Contribution of a martian atmosphere to laser-induced breakdown spectroscopy (LIBS) data and testing its emission characteristics for normalization applications. Icarus doi:10.1016/j.icarus.2019.02.017.

Shabanov, S.V., Gornushkin, I.B., 2015. Modeling chemical reactions in laser-

induced plasmas. Applied Physics A: Materials Science and Processing 121, 1087–107. doi:10.1007/s00339-015-9445-0.

Shabanov, S.V., Gornushkin, I.B., 2016. Anions in laser-induced plasmas. Applied Physics A: Materials Science and Processing 122, 676. doi:10.1007/s00339-016-0175-8.

Vogt, D.S., Rammelkamp, K., Schröder, S., Hübers, H.W., 2018. Molecular emission in laser-induced breakdown spectroscopy: An investigation of its suitability for chlorine quantification on Mars. Icarus 302, 470–82. doi:10.1016/J.ICARUS.2017.12.006.

Wiens, R.C., Maurice, S., Barraclough, B., Saccoccio, M., Barkley, W.C., Bell, J.F., Bender, S., Bernardin, J., Blaney, D., Blank, J., Bouyé, M., Bridges, N., Bultman, N., Caïs, P., Clanton, R.C., Clark, B., Clegg, S., Cousin, A., Cremers, D., Cros, A., Deflores, L., Delapp, D., Dingler, R., D'Uston, C., Darby Dyar, M., Elliott, T., Enemark, D., Fabre, C., Flores, M., Forni, O., Gasnault, O., Hale, T., Hays, C., Herkenhoff, K., Kan, E., Kirkland, L., Kouach, D., Landis, D., Langevin, Y., Lanza, N., Larocca, F., Lasue, J., Latino, J., Limonadi, D., Lindensmith, C., Little, C., Mangold, N., Manhes, G., Mauchien, P., McKay, C., Miller, E., Mooney, J., Morris, R.V., Morrison, L., Nelson, T., Newsom, H., Ollila, A., Ott, M., Pares, L., Perez, R., Poitrasson, F., Provost, C., Reiter, J.W., Roberts, T., Romero, F., Sautter, V., Salazar, S., Simmonds, J.J., Stiglich, R., Storms, S., Striebig, N., Thocaven, J.J., Trujillo, T., Ulibarri, M., Vaniman, D., Warner, N., Waterbury, R., Whitaker, R., Witt, J., Wong-Swanson, B., 2012. The ChemCam instrument suite on the Mars Science Laboratory

(MSL) rover: Body unit and combined system tests. Space Science Reviews 170, 167–227. doi:10.1007/s11214-012-9902-4.

Wiens, R.C., Maurice, S., Perez, F.R., 2017. The SuperCam Remote Sensing Instrument Suite for the Mars 2020 Rover: A Preview. Spectroscopy 32, 50–5.

Yalçin, Ş., Crosley, D.R., Smith, G.P., Faris, G.W., 1999. Influence of ambient conditions on the laser air spark. Applied Physics B: Lasers and Optics 68, 121–30. doi:10.1007/s003400050596.